Versatile Control of Unidirectional AC–DC Boost Converters for Power Quality Mitigation

Sung Min Park, *Member, IEEE*, and Sung-Yeul Park, *Member, IEEE*

***Abstract*—This paper introduces a versatile control scheme for unidirectional ac–dc boost converters for the purpose of mitigating grid power quality. Since most power factor correction circuits available in the commercial market utilize unidirectional ac–dc boost converter topologies, this is an almost no-cost solution for compensating harmonic current and reactive power in residential applications. Harmonic current and reactive power compensation methods in the unidirectional ac–dc boost converter are investigated. The additional focus of this paper is to quantify the input current distortions by the unidirectional ac–dc boost converter used for supplying not only active power to the load but also reactive power. Due to input current distortions, the amount of reactive power injected from an individual converter to the grid should be restricted. Experimental results are presented to validate the effectiveness of the proposed control method.**

***Index Terms*—Active power filter (APF), cusp distortion, harmonic current compensation (HCC), power factor correction (PFC), reactive power compensation (RPC), unidirectional ac–dc boost converter.**

I. Introduction

POWER quality analysis in ac power systems is concerned with deviations of the voltage or current from the desired ideal sinusoid of constant amplitude and frequency [1]. Unfiltered harmonics cause interferences in other electric facilities, creating abnormal and undesirable behavior of electrical equipment and transformer overheating [2]. Uncontrolled reactive power increases transmission conduction losses and deteriorates the performance of voltage regulation [3]. Therefore, it is desired to reduce these effects through adequate means, i.e., harmonic current compensation (HCC) and reactive power compensation (RPC) [2]–[5].

Several technologies, typically having high power capacities, based on power electronics theory have aimed to improve grid power quality and compensate reactive power at the transmission and distribution system level. Flexible alternating current transmission systems (FACTS) have been studied by industrial and academic researchers since 1990s [6], [7]. Alternating current transmission systems incorporating power electronics-based compensators and other static controllers generally enhance controllability and increase power transfer capability. Among FACTS technologies, the static VAR compensator (SVC), static synchronous compensator (STATCOM), and unified power quality conditioner (UPQC) all possess the capacity to compensate reactive power [7]–[11]. Active power filters (APFs) configurable with various power topologies can be utilized for improving power quality through HCC and RPC [2], [5], [12], [13]. Although SVCs, STATCOMs, UPQCs, and APFs exhibit outstanding performance, they may not be the best solution for improvement of power quality of an entire power system due to high capital and operating costs, as well as additional power losses due to long distance transmission of reactive power.

To find more economical solutions, the demands of power quality mitigation have continuously encouraged power electronics engineers to include HCC and RPC capabilities as ancillary services in bidirectional power converters [14], [15]. As power converters for renewable energy sources become more popular in ac power systems, the potential for HCC and RPC will increase, as these control schemes can be employed in existing topologies without hardware changes. Despite the increased utility and cost savings, the number of renewable power converters capable of fulfilling these functions is still limited.

Alternatively, vehicle-to-grid (V2G) technology has recently emerged for incorporation of electric vehicles (EVs) into the electric grid as energy storage units [16], [17], which can provide power quality mitigation as an ancillary service. This will result in enhanced reliability and performance of the power system. However, V2G connections require a bidirectional power converter [16]–[18], which increases system cost and complexity compared to that of a unidirectional power converter. For this reason, a unidirectional topology is a preferable configuration for level 1 battery chargers in EV and plug-in electric vehicle (PHEV) applications, meant for residential interconnections, whereas V2G utilizing bidirectional converters is more applicable for level 2 battery chargers [18].

The purpose of this paper is to investigate a cost-effective power quality mitigation solution by utilizing unidirectional converters [19], [20], even though HCC and RPC conflicts with the basic purpose and premise of maximizing the power factor. Since an immense number of these unidirectional converters are present within residential power systems, these unidirectional converters, operating in unison, have a high potential as alternative HCC and RPC units and, thus, these converters can act in place of larger, more costly HCC and RPC equipment if they possess these functionalities.

In recent years, few papers have detailed HCC and RPC functionalities using unidirectional power factor correction (PFC)

Manuscript received January 14, 2014; revised May 8, 2014 and July 8, 2014; accepted October 4, 2014. Date of publication October 22, 2014; date of current version April 15, 2015. Recommended for publication by Associate Editor R. Redl.

The authors are with the Department of Electrical and Computer Engineering, University of Connecticut, Storrs, CT 06268 USA (e-mail: sungmin.park@engr.uconn.edu; supark@engr.uconn.edu).

Color versions of one or more of the figures in this paper are available online at http://ieeexplore.ieee.org.

Digital Object Identifier 10.1109/TPEL.2014.2364304

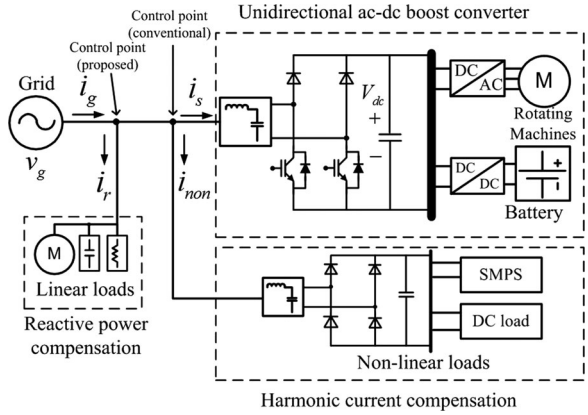

Fig. 1. Proposed system connected to linear and nonlinear loads.

converters in [16], [21], and [22]. In [16], authors broadly reviewed battery charger topologies used for EV/PHEV applications for providing reactive power support to the grid, but the RPC capability in unidirectional converters was mentioned briefly and any further analysis was not conducted. In [21], the feasibility of HCC functionality using a boost converter was presented as a low-cost solution, but RPC functionality was not mentioned. In [22], the reactive power support capabilities of the unidirectional converter within V2G applications were studied through simulation results, but detailed analysis regarding input current distortions was not performed.

In this paper, the feasibility and limitations of the unidirectional ac–dc boost PFC converter, when it is employed for HCC and RPC, are explored. In addition, an approach for estimating the distortion levels of the current under RPC modes is analytically justified. This paper starts with descriptions of control modes and analysis of local loads for the proposed system in Section II. The distortion levels on the input currents when the unidirectional ac–dc boost converter is employed for RPC are analytically explained in Section III. Experimental results are presented in order to validate the proposed approach in Section IV. Finally, Section V concludes the paper.

II. Control Mode

The dual boost PFC converter [23]–[26], often called the bridgeless PFC converter, is one of the most popular unidirectional ac–dc boost converters. The control algorithms of the dual boost PFC converter are almost identical to any conventional ac–dc converter using a diode rectifier and step-up chopper, except that the dual boost PFC converter controls ac input current, while the conventional one controls rectified output current. Fig. 1 shows a prevalent application of unidirectional ac–dc boost converters. Conventional PFC converters consider the input current to be a purely sinusoidal waveform, which is completely in phase with the input voltage. The proposed control method can ameliorate harmonic current and reactive power for improved grid power quality, as well as regulation of dc-bus voltage. The proposed versatile control of unidirectional ac–dc boost converter has three modes of operation, i.e., PFC, HCC, and RPC. Also, both HCC and RPC can operate simultaneously

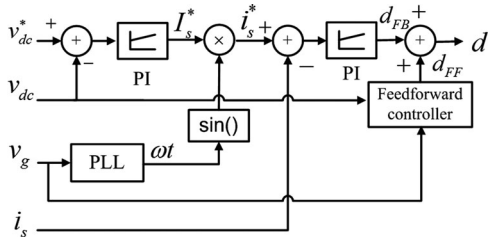

Fig. 2. Conventional control algorithm for unidirectional ac–dc boost converters.

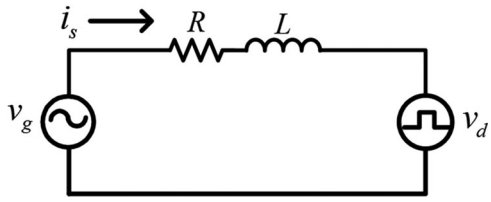

Fig. 3. Simple circuit diagram during a positive half period of the source voltage.

to improve the distortion and the displacement factors of the grid current.

A. PFC Control

PFC control methods are very common in the related literature, especially those utilizing feedback and feedforward controllers, [27], [28], as shown in Fig. 2. Fig. 3 depicts a simple circuit diagram of unidirectional ac–dc boost converters with an input inductor *L* and its parasitic resistor *R*. Kirchhoff's voltage law with the source voltage v_g, the switch voltage v_d, and the input line current yields to

$$v_g = Ri_s + L\frac{di_s}{dt} + v_d \tag{1}$$

where v_g is the instantaneous value of the source voltage expressed as $V_g \sin(\omega t)$. The switch voltage is always a major factor in determining the waveform of the input current. In other words, when producing a sinusoidal input current, the switch voltage has to emulate the source voltage identically, with the exact phase difference due to input impedance. The average switch voltage over a switching cycle in continuous conduction mode can be expressed as

$$v_d = (1-d)v_{\rm dc} \tag{2}$$

where *d* is the average on-time duty ratio of the switches and $v_{\rm dc}$ is the dc output voltage. When the source voltage is in the negative half period, the sign of the input current and switch voltage will be opposite in (1). Therefore, the source voltage can be considered as a rectified voltage, which can be expressed by the absolute sign. This indicates that the bridgeless PFC converter is identical to the general boost converter, using the single switch in rectified dc link, with regard to its operational principle. Combining (1) and (2), and rearranging in terms of *d*,

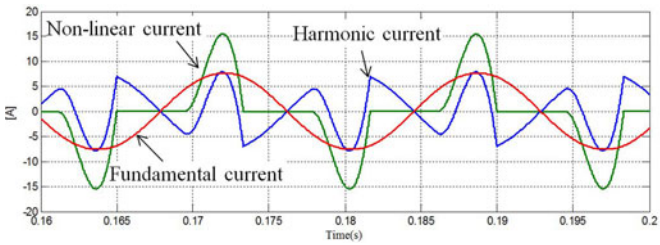

Fig. 4. Example of nonlinear load current (THD: 80%, PF: 0.705, P: 550 W, Q: 200 Var).

the duty ratio equation can be obtained as

$$d = \underbrace{\frac{1}{v_{\rm dc}}\left(Ri_s + L\frac{di_s}{dt}\right)}_{d_{\rm FB}} + \underbrace{\left(1 - \frac{|v_g|}{v_{\rm dc}}\right)}_{d_{\rm FF}}. \quad (3)$$

Theoretically, the duty ratio in (3) should be generated for the ideal switch voltage as accurately as possible through adequate converter compensators to yield sinusoidal input current. In order to classify the duty ratio d of the system in (3), the feedback duty ratio $d_{\rm FB}$ and the feedforward duty ratio $d_{\rm FF}$ can be considered separately. $d_{\rm FB}$ produces the exact phase difference between the source voltage and the average switch voltage. $d_{\rm FF}$ produces the inverse of the source voltage waveform as the average switch voltage. Hence, the input current tracking is improved and the frequency range for which input admittance acts purely as a resistance can be extended to higher frequencies due to feedforward control [27], [28].

B. Harmonic Current Compensation

Fig. 4 shows the current waveform of a typical nonlinear load in a single-phase diode rectifier. Generally, the distorted load current $i_{\rm non}$ can be written in terms of its fundamental $i_{\rm fn}$ and harmonic $i_{\rm hn}$ components as

$$i_{\rm non} = I_1 \sin(\omega_1 t + \theta_1) + \sum_{n=2,3}^{\infty} I_n \sin(n\omega_1 t + \theta_n) \quad (4)$$

where ω_1 is the line angular frequency and θ_n is the phase difference between the source voltage and input current. Assume that the input current from the unidirectional ac–dc boost converter operating in PFC mode is a purely sinusoidal waveform. The grid current i_g includes $i_{\rm hn}$ from a nonlinear load as shown in Fig. 5(a). These harmonics are undesirable and should be removed. If the unidirectional ac–dc boost converter can generate the harmonic current capable of canceling the harmonics of the nonlinear load, the grid current will be comprised of only fundamental components of the converter current and load current as shown in Fig, 5(b). Therefore, the new current reference for the current controller of the converter from Fig. 6 can be expressed as

$$i_s^* = I_s^* \sin(\omega t) - i_{\rm hn} \quad (5)$$

where I_s^* is the magnitude reference provided by the dc-bus voltage controller.

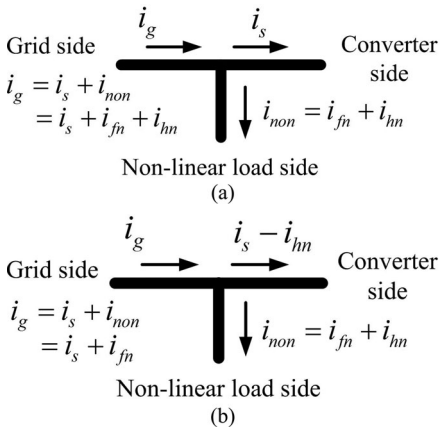

Fig. 5. Harmonic current flow diagram (a) without HCC and (b) with HCC.

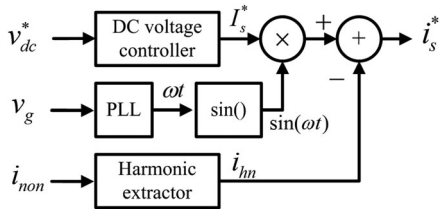

Fig. 6. Current reference generator block for HCC.

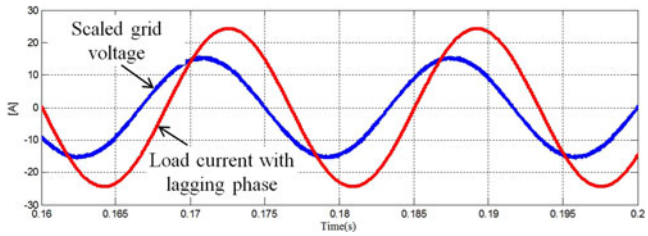

Fig. 7. Example of linear load current (THD: 0.5%, PF:0.8, active power: 1500 W, reactive power: 1100 Var).

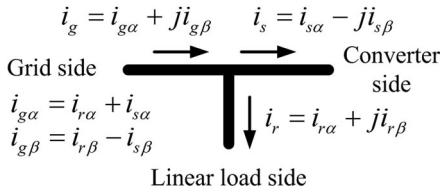

Fig. 8. Current flow diagram in RPC mode at the PCC.

C. Reactive Power Compensation

Unlike nonlinear loads, the current waveform of a linear load is sinusoidal at the frequency of the power system [1], but the power factor can be significantly exacerbated when the load is capacitive or inductive. Fig. 7 shows the current waveform of a typical inductive load in a single-phase induction motor. The current flow, consisting of the converter current with RPC and the load current i_r consuming reactive power, shown in Fig. 8,

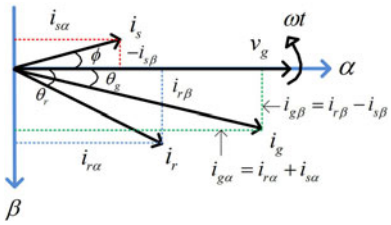

Fig. 9. Phase diagram of the grid voltage and current during RPC.

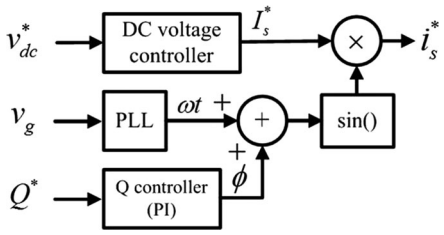

Fig. 10. Current reference generator block for RPC.

can be written, respectively, as

$$i_s = i_{s\alpha} - j i_{s\beta} \tag{6}$$

$$i_r = i_{r\alpha} + j i_{r\beta} \tag{7}$$

$$i_g = i_{r\alpha} + i_{s\alpha} + j(i_{r\beta} - i_{s\beta}). \tag{8}$$

As a result, the grid power factor at the PCC can be improved by injecting reactive power from the converter as shown in Fig. 9. However, it should be considered that the input current of the unidirectional converter becomes distorted due to the natural commutation of diodes; thus, the amount of reactive power generated by an individual converter should be restricted [22], [29]. This will be elaborated later in this paper. Since the current waveform of the converter in RPC mode is not sinusoidal, the required phase angle of the current cannot be calculated by a simple reactive power equation. Thus, the phase angle reference to the input converter current needs to be generated by employing a proportional integral compensator as shown in Fig. 10, and can be represented as

$$\phi = K_{pc}(Q^* - Q) + K_{ic} \int (Q^* - Q) dt \tag{9}$$

$$i_s^* = I_s^* \sin(\omega t + \phi) \tag{10}$$

where $K_{\rm pc}$ and $K_{\rm ic}$ are proportional gain and integral gain of the reactive power compensator, respectively, and ϕ is the desired phase to be adjusted from the original current reference. It should be noted in (10) that the current magnitude reference I_s^* will be adjusted through the dc-bus voltage controller to feed active power to the dc load. The reactive power will be adjusted by changing the phase angle ϕ. Thus, initially I_s^* is determined by the dc-link voltage controller and actual active power will change as result of generating reactive power with respect to the dc link command. However, since I_s^* will be updated by the dc link voltage compensator, as the phase angle ϕ changes, the dc link voltage will be maintained.

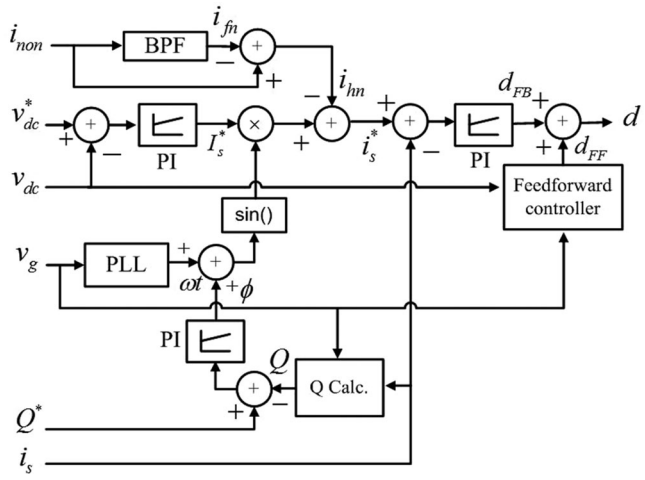

Fig. 11. Proposed HCC and RPC control block diagram.

D. Control Strategy for APF Functionality

The proposed control strategy of the unidirectional ac–dc converter including a feedforward controller, HCC, and RPC is shown in Fig. 11. Two control blocks for HCC and RPC have been added to the conventional control algorithm in Fig. 2. Thus, the final current reference for a versatile control strategy based on (5) and (10) can be expressed as

$$i_s^* = I_s^* \sin(\omega t + \phi) - i_{\rm hn}. \tag{11}$$

In addition, it is worthwhile to mention that functionalities of HCC and RPC in unidirectional ac–dc boost converters are available only when these converters supply active power to its dc load. Thus, the current reference able to be used for HCC and RPC is highly dependent on its power rating and its existing loads. Since multiple unidirectional converters may be connected to the power system in residential applications, their RPC capabilities can be maximized by incorporating these aggregated converters as shown in Fig. 12. The possible supervisory control strategy for future smart grid applications [30] can be suggested as follows:

1) analyze grid power quality factors, such as THD and PF;
2) calculate the amount of compensation for harmonic producing components and reactive power;
3) obtain the available capacities used for HCC and RPC in an individual converter;
4) determine and distribute HCC and RPC references to an individual converter;
5) analyze the grid power quality. If the THD of the grid current is above 5%, the level of RPC needs to be reduced, otherwise, the amount of RPC can be increased up to each converter's maximum capacity to achieve unity power factor.
6) repeat (1) through (5).

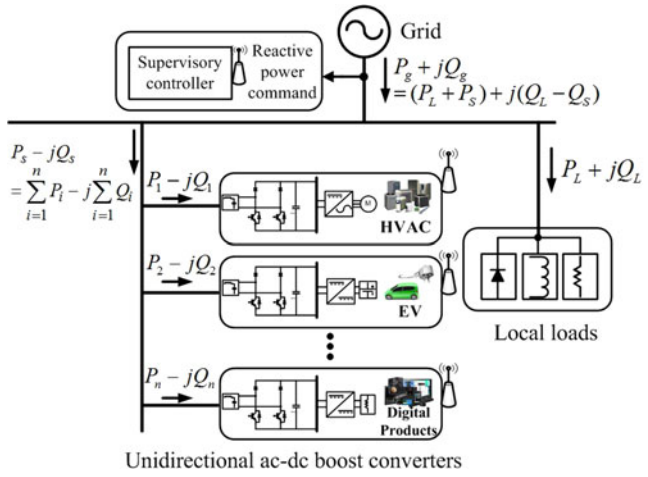

Fig. 12. RPC using aggregated unidirectional ac–dc boost converters.

Using these steps, the grid power quality can be enhanced, as long as the available converter capacities for HCC and RPC remain.

III. Analysis and Estimation of Current Distortion

In the conventional control method of unidirectional ac–dc boost converters, the magnitude and phase of the current reference can be obtained in the dc-voltage controller and the phase-locked loop (PLL), respectively. By adjusting the phase angle ϕ in (10), the current either leads or lags in reference to the voltage. This allows the generation or consumption of reactive power in unidirectional ac–dc boost converters. Due to the intrinsic operation of diodes, however, uncontrolled regions exist, where the signs of the input voltage and current reference are opposite [31] and the actual current in unidirectional converters is not capable of following the current reference exactly. Therefore, an analytical approach is required to estimate current distortions and actual generated power. To simplify and generalize the current waveform in this paper, it is assumed that the duty output from the controller is zero in these regions.

A. Extended Cusp Distortion in the Capacitive Current

Fig. 13(a) depicts the comparison of the current waveforms during capacitive power compensation. It can be observed in Fig. 13(b) that there are two distortion periods: the zero-current distortion and the cusp distortion regions. Due to the unidirectional power flow capabilities of the converter, the current is periodically uncontrollable when signs of the input voltage and current reference are opposite, which creates the zero-current distortion region ϕ. In addition, the current drastically increases after the grid voltage crosses zero, which leads to the cusp distortion common to all PFC circuits using boost converter configurations [32]. This occurs because the inductor voltage is limited in its ability to drive its current up, even with the switch closed during this time [31].

It should be noted in Fig. 13(b) that the duration of the cusp distortion is extended up to t_c in capacitive power compensation,

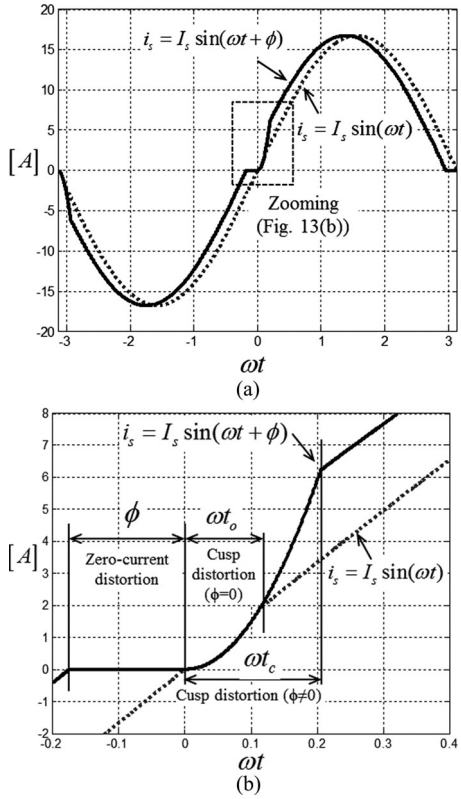

Fig. 13. Capacitive power compensation in a unidirectional ac–dc boost converter. (a) Comparison of current wavefoms. (b) Zero current and cusp distortion in zoomed regions.

compared to the original t_o in unity power factor mode. Since the switch is always ON during the cusp distortion ($d = 1$ in this condition), only the source voltage and inductor voltage remain in Fig. 3, i.e., the averaged source voltage is zero. Therefore, the input current is described by

$$i_s(t) = \frac{V_g}{L}\int_0^{t_c} \sin(\omega t)dt = \frac{V_g}{X}(1 - \cos(\omega t_c)) \tag{12}$$

where $X = \omega L$ and V_g is the peak input voltage. The cusp distortion continues until the actual current meets the capacitive current reference

$$\frac{V_g}{X}(1 - \cos(\omega t_c)) = I_s \sin(\omega t_c + \phi). \tag{13}$$

By solving (13) in terms of ωt_c, the extended duration of the cusp distortion ωt_c can be calculated as

$$\omega t_c = \tan^{-1}\left(\frac{\sqrt{X^2 I_s^2 + 2V_s I_s X \sin\phi}}{V_g}\right) + \tan^{-1}\left(\frac{I_s \cos\phi}{I_s \sin\phi + V_g/X}\right) \tag{14}$$

ωt_o can be obtained as $2\tan^{-1}(XI_s/V_g)$ when ϕ is zero in (14), which corresponds with [32]. Fig. 14(a) shows ωt_c values calculated by (14) with various inductances L under v_g is 110 $V_{\rm rms}$. It increases in magnitude as the inductance value and peak current increase. Additionally, ωt_c is prolonged, as shown

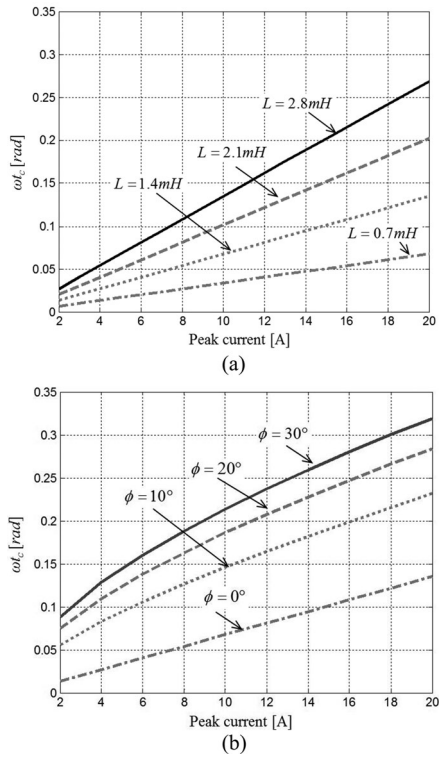

Fig. 14. Duration of the cusp distortion in various L values and capacitive currents. (a) ωt_c versus peak current for different L values when $\phi = 0$. (b) ωt_c versus peak current for different ϕ when $L = 1.4$ mH.

in Fig. 14(b), when more capacitive current is required because the current error between the actual current and reference current after the zero crossing of the input voltage grows.

B. Analysis of the Capacitive Current

Based on periods of zero current and cusp distortions, the resulting current waveform in capacitive power compensation can be defined by

$$i_s(t) = \begin{cases} \frac{V_s}{X}(1-\cos(\omega t)), & 0 \le \omega t < \omega t_c \\ I_s \sin(\omega t + \phi), & \omega t_c \le \omega t < \pi - \phi \\ 0, & \pi - \phi \le \omega t < \pi \\ \frac{V_s}{X}(-1-\cos(\omega t)), & \pi \le \omega t < \pi + \omega t_c \\ I_s \sin(\omega t + \phi), & \pi + \omega t_c \le \omega t < 2\pi - \phi \\ 0, & 2\pi - \phi \le \omega t < 2\pi. \end{cases} \tag{15}$$

Even though the current reference in (10) is used to generate or consume reactive power, the real current is not capable of tracking the current reference in an exact manner due to the zero current and extended cusp distortions. Since the real currents are distorted, the fundamental current needs to be extracted to calculate the actual active and reactive power. According to the Fourier series, the current waveform in (15) can be expressed as the sum of multiple sinusoids of different frequencies [1]

$$i_s(t) = a_0 + \sum_{n=1}^{\infty} [a_n \cos n\omega t + b_n \sin n\omega t] \tag{16}$$

where a_o is the dc value (zero under a perfect ac waveform, i.e., $a_o = 0$), a_n and b_n are the amplitudes of the *n*th cosine-term and sine-term harmonics, respectively. Regarding the fundamental content of the capacitive current in (15), the Fourier series coefficient at the fundamental frequency can be solved as

$$a_1 = \frac{1}{2\pi}\begin{pmatrix} I_s(\cos(\phi + 2\omega t_c) - \cos\phi \\ +2(\pi - \phi - \omega t_c)\sin\phi) \\ -\frac{V_s}{X}(\sin(2\omega t_c) - 4\sin(\omega t_c) + 2\omega t_c) \end{pmatrix} \tag{17}$$

$$b_1 = \frac{1}{2\pi}\begin{pmatrix} I_s(\sin(\phi + 2\omega t_c) + \sin\phi \\ +2(\pi - \phi - \omega t_c)\cos\phi) \\ +\frac{2V_s}{X}(\cos(\omega t_c) - 1)^2. \end{pmatrix} \tag{18}$$

Using (17) and (18), the current with the fundamental radian frequency ω can be obtained as

$$i_{s1} = I_{s1}\sin(\omega t + \delta) \tag{19}$$

where $I_{s1} = \sqrt{a_1^2 + b_1^2}, \delta = \tan^{-1}(a_1/b_1)$

It should be noted that δ is a displacement angle in the current in reference to the fundamental frequency, which contributes to the production of actual active and reactive power, rather than just at the phase angle reference (ϕ). The rms value of the current waveform in (15) can be defined and calculated as

$$\begin{aligned} I_{s\text{rms}} &= \sqrt{\frac{1}{2\pi}\int_0^{2\pi} i_s^2(t)dt} \\ &= \sqrt{\frac{1}{4\pi}\begin{pmatrix} I_s^2(2(\pi - \phi - \omega t_c) + \sin(2\phi + 2\omega t_c)) \\ +\frac{V_s^2}{X^2}(6\omega t_c + \sin(2\omega t_c) - 8\sin(\omega t_c)) \end{pmatrix}} \end{aligned} \tag{20}$$

Using rms values of the fundamental and total current from (19) and (20), the theoretical THD values of the input current under RPC can be obtained as

$$\text{THD}_{\text{th}} = \frac{\sqrt{I_{s\text{rms}}^2 - I_{s1\text{rms}}^2}}{I_{s1\text{rms}}} \tag{21}$$

where $I_{s1\text{rms}} = \frac{\sqrt{a_1^2 + b_1^2}}{\sqrt{2}}$.

In addition, the active and reactive power under RPC can be calculated as

$$P = \frac{1}{2}V_s I_{s1}\cos\delta \tag{22}$$

$$Q = -\frac{1}{2}V_s I_{s1}\sin\delta. \tag{23}$$

Finally, using (21)–(23), the theoretical THD values and the expected active and reactive power in capacitive power compensation mode can be calculated as shown in Fig. 15. It can be noted that not only the zero-current distortion, but also the cusp distortion causes the current distortion level to increase at higher capacitive power.

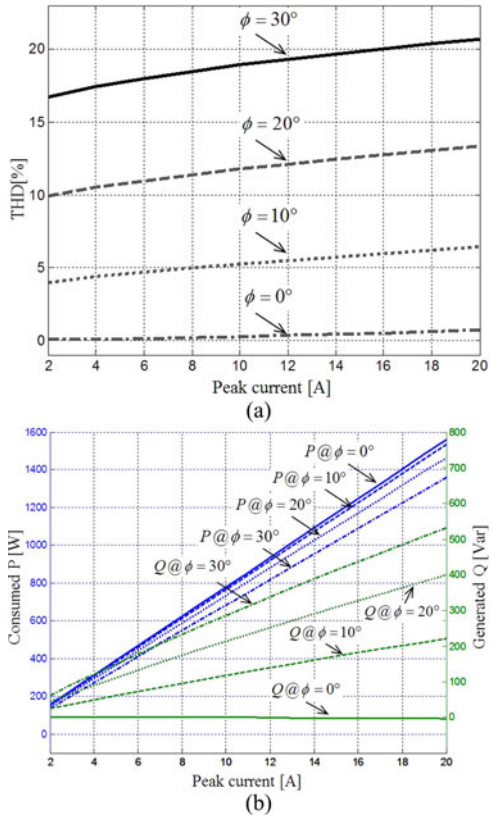

Fig. 15. Analytical results in capacitive power compensation mode. (a) THD versus peak current for different ϕ. (b) Active power and reactive power versus peak current for different ϕ.

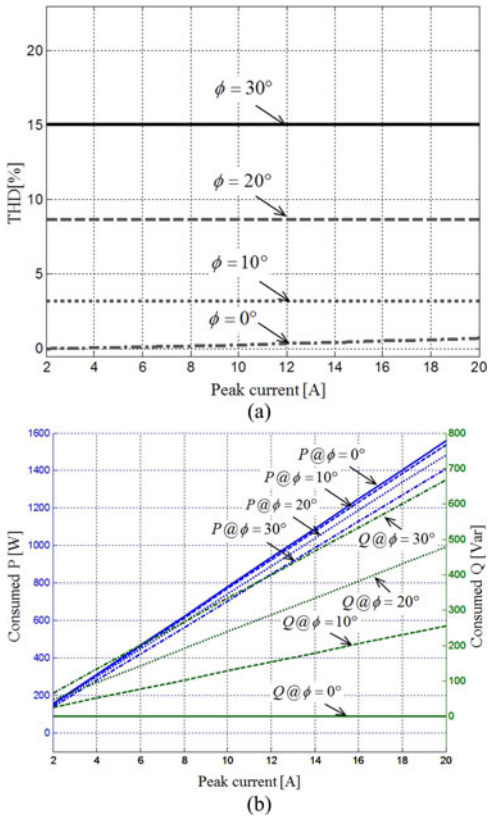

Fig. 17. Analytical results in inductive power compensation mode. (a) THD versus peak current for different ϕ. (b) Active power and reactive power versus peak current for different ϕ.

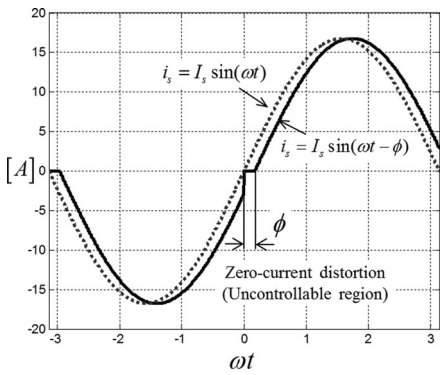

Fig. 16. Current waveforms in inductive power compensation.

C. Analysis of the Inductive Current

Similarly, Fig. 16 depicts the comparison of the current waveforms with varying inductive power. Compared to the capacitive current, the cusp distortion is not as pronounced because the voltage across the boost inductor is already high enough to drive the required current. However, in this scenario, the zero-current distortion still appears due to the uncontrollable regions caused by the diodes. The resulting current waveform for inductive power compensation is simpler than the capacitive current, and can be defined as

$$i_s(t) = \begin{cases} 0, & 0 \le \omega t < \phi \\ I_s \sin(\omega t - \phi), & \phi \le \omega t < \pi \\ 0, & \pi \le \omega t < \pi + \phi \\ I_s \sin(\omega t - \phi), & \pi + \phi \le \omega t < 2\pi. \end{cases} \tag{24}$$

Deriving the Fourier series coefficients in the same way, and expressing the rms values of the current with respect to the fundamental frequency

$$a_1 = \frac{-I_s\,(\pi - \phi)\sin\phi}{\pi} \tag{25}$$

$$b_1 = \frac{I_s}{\pi}(\sin\phi + (\pi - \phi)\cos\phi) \tag{26}$$

$$I_{s\mathrm{rms}} = \sqrt{\frac{I_s^2}{4\pi}(2(\pi - \phi) + \sin(2\phi))}. \tag{27}$$

Equations (25) and (26) are used to obtain the fundamental current in (19), substituting its outcome and (27) into (21)–(23) yields the expected values of the THD, active power, and reactive power in inductive power compensation, as shown in Fig. 17. It is notable that the distortion level remains unchanged regardless of the magnitudes of the current, but deteriorates as ϕ increases. The currents in inductive power compensation, when compared to the currents in capacitive power compensation, exhibit approximately a 30% reduction of THD. For example,

when ϕ is 20°, the THD values of the capacitive and inductive currents at 17 A are 12.9% and 8.7%, respectively, because the inductive current does not have cusp distortions. As a result, inductive power compensation yields a higher amount of reactive power (when only absolute values of reactive power are compared) at the same phase angle when Figs. 15(b) and 17(b) are compared.

The grid current THD highly depends on load currents and converter currents. If the load power is much greater and more sinusoidal than that of the converter, the grid current THD is less affected by the converter current distortion when RPC is enabled and vice versa. If there is no load current, the grid current is identical to the converter current. Since the converter current THD is dependent on many electrical parameters such as the grid voltage, converter power rating, and maximum shifted phase angle, each converter has different RPC capabilities even if the power rating of the converter is similar with others. From Figs. 15(a) and 17(a), the maximum shifted phase angle, which should not cause current THD higher than 5%, can be estimated. Then, using its maximum shifted phase angle and converter power ratings, the maximum reactive power can be estimated theoretically in Figs. 15(b) and 17(b). In conclusion, approximately up to 15% and 30% of available power from a 1.2-kVA unidirectional converter can be supplied for capacitive and inductive power, respectively. From a single converter, this capability is relatively small, but RPC capabilities can be multiplied by utilizing aggregated unidirectional converters as shown in Fig. 12.

D. Discussion About THD Estimation

Although the current distortion levels based on the emulated current models in (15) and (24) are mathematically predicted in previous sections, actual distortion levels under practical implementations might deviate from these theoretical results because the quality of current waveforms correlate closely with many hardware and software components, such as the performances of the current compensator, filters, and PLL, as well as the noise immunity of the sensors and the linearity of the inductor [33]. Due to these inherent imperfections, commercial ac–dc PFC converters in unity power factor mode ordinarily have THD values in the range of 2% to 5%. Since this imperfection from real circuits relates to the real current waveforms of the converter, it also affects THD values of reactive power current and causes the deviation between the theoretical and actual THD values. Therefore, the actual THD considering this deviation can be represented approximately as

$$\mathrm{THD}_{\mathrm{com}} \approx \mathrm{THD}_{\mathrm{th}} + \mathrm{THD}_{\mathrm{dev}} \tag{28}$$

where $\mathrm{THD}_{\mathrm{th}}$ is the theoretical THD value from (21), and $\mathrm{THD}_{\mathrm{dev}}$ is an averaged deviation based on experimental results in unity power factor mode. In this paper, $\mathrm{THD}_{\mathrm{dev}}$ 2.14% will be used for calculating the estimated THD in (28).

IV. Experimental Results

A 700-W dual boost PFC converter was implemented in order to validate the proposed system. The passive and electronic loads used as linear and nonlinear loads are connected with the grid and converter at the PCC. Fig. 18 shows the experimental test bench and Table I lists some important experimental values.

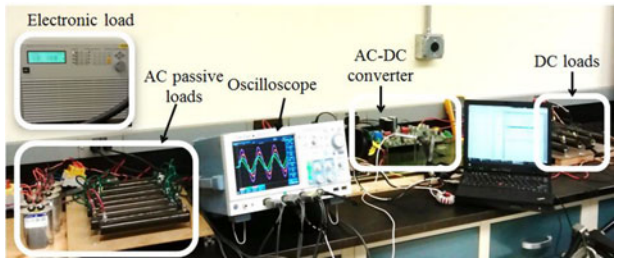

Fig. 18. Test bench setup.

TABLE I
Experimental Setup

System parameter	Values
AC Source Voltage	110 Vrms / 60Hz
Rated Power	700 W
Switching Frequency	20 kHz
Boost Inductor	1.4 mH (split into two in series)
DC capacitor	2040 μF
DSP	TMS320F28035 (TI)
Power device	FPDB60PH60B (FAIRCHILD)
Grid emulator	3120-AMX (PACIFIC)
Load emulator	63803 (CHROMA) and *RLC* loads

A. Estimating Current Distortion Levels

The estimated, simulated, and measured output current and grid voltage waveforms in different operation modes are presented in Figs. 19 and 20 as an example to show the effectiveness of the proposed approach for estimating current distortion levels in RPC mode, where the peak current and phase references are 17 A and 20°, respectively. The waveforms of measured currents are nearly identical to the waveforms of the estimated and simulated results. In agreement with the analytical results, the capacitive current suffers from the zero current and cusp distortions as shown in Fig. 19, whereas the inductive current, as shown in Fig. 20, is distorted only by the zero-current distortion.

Fig. 21 shows test results comparing the measured THD values with the estimated values. The THD differences between the estimated THD from (28) and measured THD values from experimental tests are below 1% and the total averaged THD difference is approximately 0.3%. In addition, it can be observed clearly that the measured THD values in capacitive power compensation mode tend to increase as the peak current and shifted-phase-angle increase, whereas the measured THD values in inductive power compensation are inclined to be constant regardless of the magnitude of the current at a fixed phase angle. These features match the previous analytical results. Hence, the experimental results demonstrate that the proposed analytical approach is an effective solution for estimating current

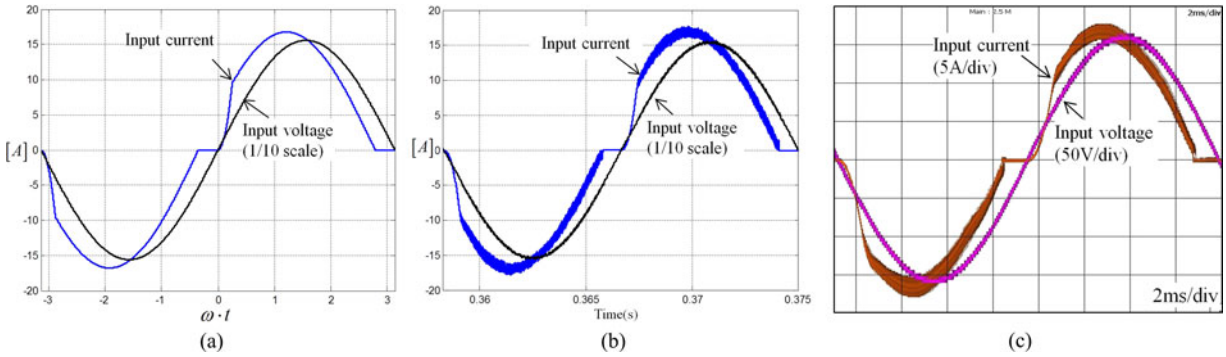

Fig. 19. Comparison of waveforms in capacitive power compensation ($I_s^* = 17$ A, $\phi = 20$). (a) Estimated result ($\mathrm{THD_{com}}$: 15. 1%). (b) Simulation result (THD: 15.1%). (c) Experimental result (THD: 15.5%).

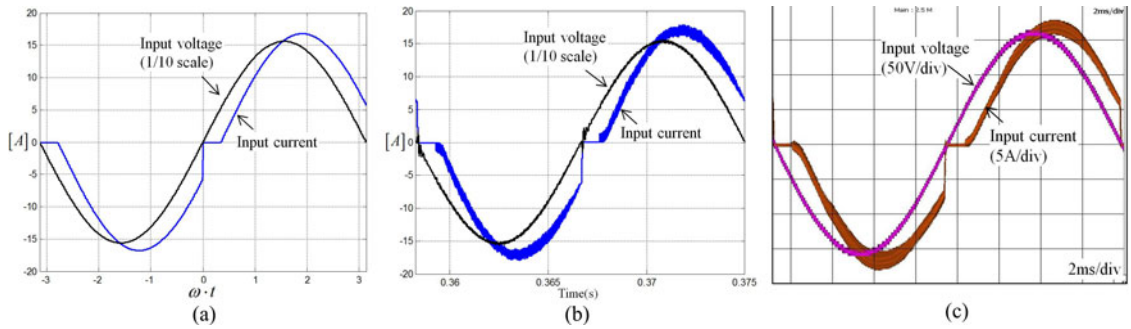

Fig. 20. Comparison of waveforms in inductive power compensation ($I_s^* = 17$ A, $\phi = 20°$). (a) Estimated result ($\mathrm{THD_{com}}$: 10.9%). (b) Simulation result (THD: 10.7%). (c) Experimental result (THD: 10.3%).

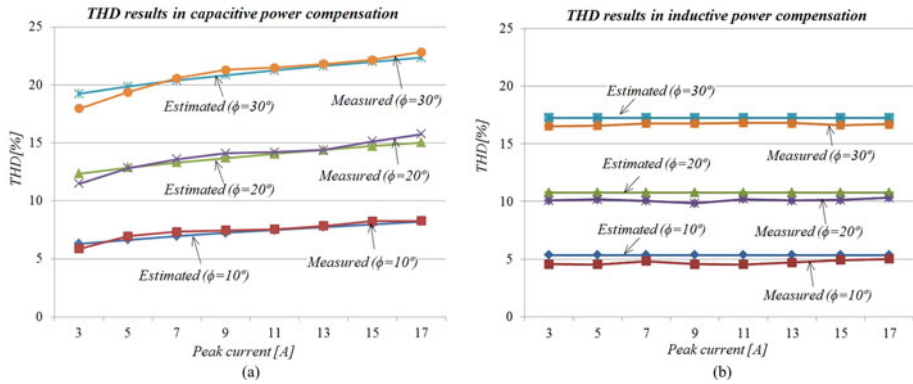

Fig. 21. Experimental results for THD of input currents. (a) Capacitive power compensation. (b) Inductive power compensation.

distortion levels in unidirectional ac–dc boost converters with RPC modes.

B. Harmonic Current Compensation

Fig. 22 shows the experimental results in HCC mode when an emulated nonlinear load with 82% THD current is connected to the unidirectional ac–dc boost converter operating at 700 W at the PCC. Before HCC mode is enabled, the converter current THD is 2.7% and the PF is 0.994, while the grid THD is polluted with the harmonic current from the nonlinear load, resulting in 15.5% THD with a peak-shape waveform as shown in Fig. 22(a). However, after HCC mode is enabled and the converter current is intentionally distorted, it can be observed that the grid current can be a sinusoidal waveform with 4.5% THD, along with improved power factor as a result of canceling the load harmonic current as shown in Fig. 22(b) and (c).

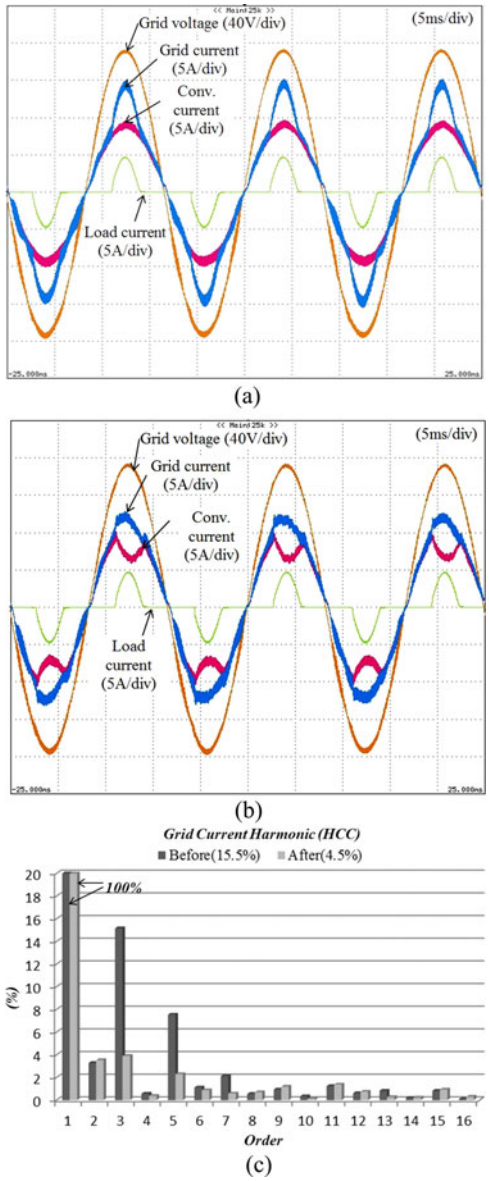

Fig. 22. Experimental results in harmonic compensation mode (a) before HCC, (b) after HCC, and (c) harmonic analysis of the grid current.

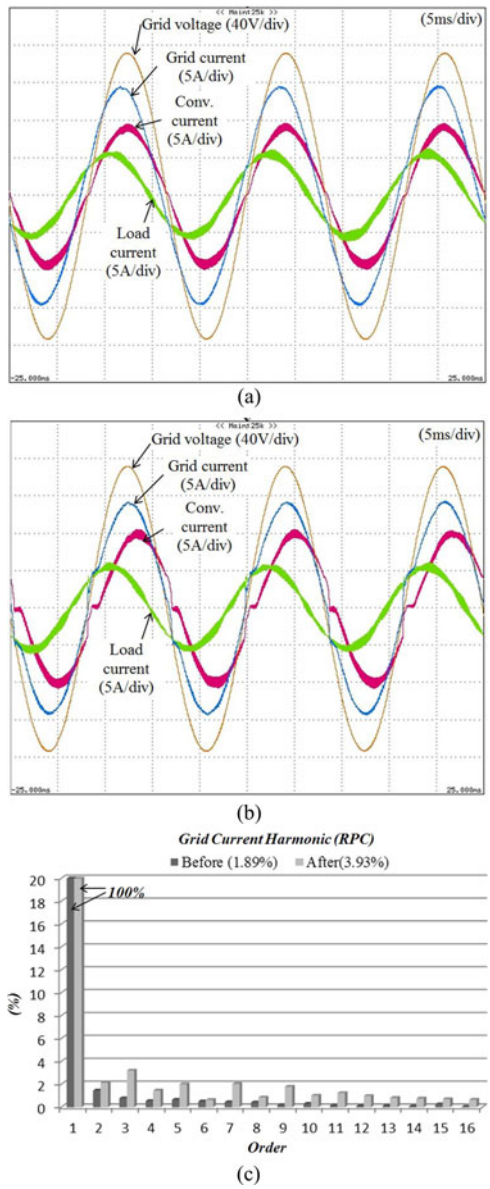

Fig. 23. Experimental results in RPC mode (a) before RPC, (b) after RPC, and (c) harmonic analysis of the grid current.

C. Reactive Power Compensation

Fig. 23 shows the experimental results in RPC mode when a passive load consisting of several resistors and capacitors connected to the unidirectional ac–dc boost converter at the PCC is used as a linear load with a poor PF of 0.779 and generating 262 Var. Before RPC mode is enabled, the grid power factor decreases to 0.963 due to this capacitive load, even under the unity power factor of the converter as shown in Fig. 23(a). After RPC mode is enabled, the converter consumes 300 Var. It can be observed that the power factor of the grid is improved from 0.963 to 0.992 as shown in Fig. 23(b). However, the THD of the grid current increases from 1.89% to 3.93% as shown in Fig. 23(c) due to inherent distortions of reactive power current in unidirectional ac–dc boost converters as explained in previous sections. Thus, the amount of reactive power used for compensation should be limited to maintain low THD of the grid current.

D. Combined Compensation Mode

Fig. 24 shows the experimental results for combined operations of HCC and RPC when the two loads used in previous experimental tests are connected at the PCC. When the converter is operating in PFC mode, the grid PF and the THD of the grid current are 0.960 and 11.2%, respectively. HCC and RPC begin simultaneously, and the resulting grid power quality improves to 0.992 PF and 4% THD at the same time. From experimental results, the grid power quality can be partially enhanced through the proposed versatile control strategy, even though a unidirectional ac–dc boost converter is implemented

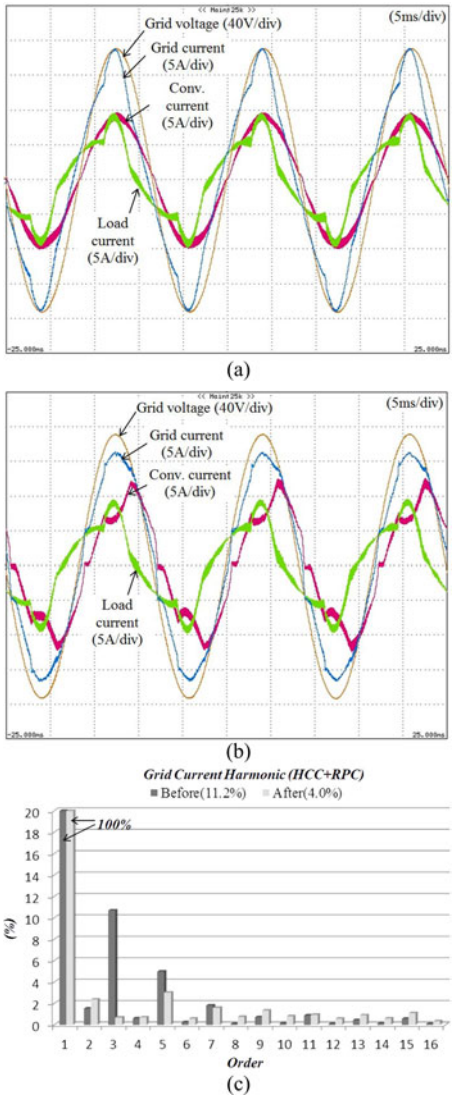

Fig. 24. Experimental results in combined HCC and RPC mode (a) before HCC and RPC, (b) after HCC and RPC, and (c) harmonic analysis of the grid current.

instead of a bidirectional converter. Experimental results under all test conditions are summarized in Table II.

V. Conclusion

Since unidirectional ac–dc boost converters are already ubiquitously connected with ac power systems, existing unidirectional ac–dc boost converters possess the ability to improve substantially the stability of ac power systems by maximizing functionalities of aggregated unidirectional ac–dc boost converters. In this paper, versatile control methods for the unidirectional ac–dc boost converter have been presented to enhance grid power quality through the combination of HCC and RPC, which can be a more economical solution for future smart grid applications. In addition, the framework for evaluation of the current distortion levels in unidirectional ac–dc boost converters when they are employed for RPC has been presented. The effectiveness of the proposed control method was validated through experimental results showing improved power factor and total harmonic distortion of the grid. At the same time, it should be noted that due to the inherent limitations of the unidirectional ac–dc boost converter, the grid current will be distorted unintentionally when operating in RPC mode where the THD of capacitive current is worse than that of the inductive current due to extended cusp distortions. Hence, the amount of reactive power injected from an individual converter to the grid should be restricted. Although, combined operation of these aggregated converters, each restricted in RPC, can meet the reactive power demand while still effectively compensating for generated harmonics.

TABLE II
Summary of Experimental Results

Mode	Items	Unidirection PFC converter		Load1 (nonlinear)	Load2 (linear)	Grid	
		Conv.	Proposed			Conv.	Proposed
HCC	P (W)	695	695	165	N/A	905	905
	Q (Var)	−20	−125	145	N/A	160	50
	THD	2.7%	17.1%	82.0%	N/A	15.5%	4.5%
	PF	0.994	0.961	0.559	N/A	0.964	0.989
RPC	P (W)	695	695	N/A	330	1067	1067
	Q (Var)	−20	300	N/A	−262	−262	75
	THD	2.7%	5.1%	N/A	0.86%	1.89%	3.93%
	PF	0.994	0.908	N/A	0.779	0.963	0.992
HCC + RPC	P (W)	695	695	490		1225	1225
	Q (Var)	−20	360	−295		−290	90
	THD	2.7%	16.2%	24.3%		11.2%	4.0%
	PF	0.994	0.870	0.824		0.960	0.992

References

[1] S. Santoso, *Fundamentals of Electric Power Quality*. Scotts Valley, CA, USA: CreateSpace, 2012.
[2] B. Singh, K. Al-Haddad, and A. Chandra, "A review of active filters for power quality improvement," *IEEE Trans. Ind. Electron.*, vol. 46, no. 5, pp. 960–971, Oct. 1999.
[3] R. Majumder, "Reactive power compensation in single-phase operation of microgrid," *IEEE Trans. Ind. Electron.*, vol. 60, no. 4, pp. 1403–1416, Apr. 2013.
[4] J. Dixon, L. Moran, J. Rodriguez, and R. Domke, "Reactive power compensation technologies: State-of-the-art review," *Proc. IEEE*, vol. 93, no. 12, pp. 1244–1264, Dec. 2005.
[5] M. El-Habrouk, M. K. Darwish, and P. Mehta, "Active power filters: A review," *Proc. Inst. Elect. Eng.—Electr. Power Appl.*, vol. 147, no. 5, pp. 403–413, Sep. 2000.
[6] N. G. Hingorani, "Flexible AC transmission," *IEEE Spectr.*, vol. 30, no. 4, pp. 40–45, Apr. 1993.
[7] N. G. Hingorani and L. Gyugyi, *Understanding FACTS: Concepts and Technology of Flexible AC Transmission Systems*. Piscataway, NJ, USA: IEEE Press, 2000.
[8] L. Gyugyi, "Power electronics in electric utilities: Static VAR compensators," *Proc. IEEE*, vol. 76, no. 4, pp. 483–494, Apr. 1988.
[9] P. S. Sensarma, K. R. Padiyar, and V. Ramanarayanan, "Analysis and performance evaluation of a distribution STATCOM for compensating voltage fluctuations," *IEEE Trans. Power Del.*, vol. 16, no. 2, pp. 259–264, Apr. 2001.
[10] S. R. Arya and B. Singh, "Performance of DSTATCOM using leaky LMS control algorithm," *IEEE J. Emerg. Sel. Topics Power Electron.*, vol. 1, no. 2, pp. 104–113, Jun. 2013.
[11] V. Khadkikar, "Enhancing electric power quality using UPQC: A comprehensive overview," *IEEE Trans. Power Electron.*, vol. 27, no. 5, pp. 2284–2297, May 2012.

[12] P. Acuna, L. Moran, M. Rivera, J. Dixon, and J. Rodriguez, "Improved active power filter performance for renewable power generation systems," *IEEE Trans. Power Electron.*, vol. 29, no. 2, pp. 687–694, Feb. 2014.
[13] R. L. de Araujo Ribeiro, C. C. de Azevedo, and R. M. de Sousa, "A robust adaptive control strategy of active power filters for power-factor correction, harmonic compensation, and balancing of nonlinear loads," *IEEE Trans. Power Electron.*, vol. 27, no. 2, pp. 718–730, Feb. 2012.
[14] M. Singh, V. Khadkikar, A. Chandra, and R. K. Varma, "Grid interconnection of renewable energy sources at the distribution level with power-quality improvement features," *IEEE Trans. Power Del.*, vol. 26, no. 1, pp. 307–315, Jan. 2011.
[15] R. I. Bojoi, L. R. Limongi, D. Roiu, and A. Tenconi, "Enhanced power quality control strategy for single-phase inverters in distributed generation systems," *IEEE Trans. Power Electron.*, vol. 26, no. 3, pp. 798–806, Mar. 2011.
[16] M. C. Kisacikoglu, B. Ozpineci, and L. M. Tolbert, "EV/PHEV bidirectional charger assessment for V2G reactive power operation," *IEEE Trans. Power Electron.*, vol. 28, no. 12, pp. 5717–5727, Dec. 2013.
[17] K.-W. Hu and C.-M. Liaw, "On a bidirectional adapter with G2B charging and B2X emergency discharging functions," *IEEE Trans. Ind. Electron*, vol. 61, no. 1, pp. 243–257, Jan. 2014.
[18] M. Yilmaz and P. T. Krein, "Review of battery charger topologies, charging power levels, and infrastructure for plug-in electric and hybrid vehicles," *IEEE Trans. Power Electron*, vol. 28, no. 5, pp. 2151–2169, May 2013.
[19] M. M. Jovanovic and Y. Jang, "State-of-the-art, single-phase, active power-factor-correction techniques for high-power applications—An overview," *IEEE Trans. Ind. Electron.*, vol. 52, no. 3, pp. 701–708, Jun. 2005.
[20] J. W. Kolar and T. Friedli, "The essence of three-phase PFC rectifier systems—Part I," *IEEE Trans. Power Electron.*, vol. 28, no. 1, pp. 176–198, Jan. 2013.
[21] N. R. Hamzah, M. K. Hamzah, A. S. Abu Hasim, and N. F. A. A. Rahman, "Single-phase shunt active power filter using single-switch incorporating boost circuit," in *Proc. IEEE Int. Power Energy Conf.*, 2008, pp. 1112–1117.
[22] M. A. Fasugba and P. T. Krein, "Gaining vehicle-to-grid benefits with unidirectional electric and plug-in hybrid vehicle chargers," in *Proc. IEEE Veh. Power Propulsion Conf.*, Sep. 2011, pp. 1–6.
[23] Y. Cho and J. Lai, "Digital plug-in repetitive controller for single-phase bridgeless PFC converters," *IEEE Trans. Power Electron.*, vol. 28, no. 1, pp. 165–175, Jan. 2013.
[24] L. Huber, Y. Jang, and M. M. Jovanovic, "Performance evaluation of bridgeless PFC boost rectifiers," *IEEE Trans. Power Electron.*, vol. 23, no. 3, pp. 1381–1390, May 2008.
[25] Y. Li and T. Takahashi, "A digitally controlled 4-kW single-phase bridgeless PFC circuit for air conditioner motor drive applications," in *Proc. CES/IEEE 5th Int. Power Electron. Motion Control Conf.*, Aug. 2006, vol. 1, pp. 1–5.
[26] A. Murray and Y. Li, "Motion control engine achieves high efficiency with digital PFC integration in air conditioner -applications," in *Proc. IEEE Int. Symp. Electron. Environ.*, 2006, pp. 120–125.
[27] M. Chen and J. Sun, "Feedforward current control of boost single-phase PFC converters," *IEEE Trans. Power Electron.*, vol. 21, no. 2, pp. 338-345, Mar. 2006.
[28] D. M. Van de Sype, K. De Gusseme, A. P. M. Van den Bossche, and J. A. Melkebeek, "Duty-ratio feedforward for digitally controlled boost PFC converters," *IEEE Trans. Ind. Electron.*, vol. 52, no. 1, pp. 108–115, Feb. 2005.
[29] S. M. Park and S.-Y. Park, "Versatile unidirectional AC-DC converter with harmonic current and reactive power compensation for smart grid applications," in *Proc. IEEE Annu. Appl. Power Electron. Conf.*, Mar. 2014, pp. 2163–2170.
[30] D. Boroyevich, I. Cvetkovic, R. Burgos, and D. Dong, "Intergrid: A future electronic energy network?" *IEEE J. Emerg. Sel. Topics Power Electron.*, vol. 1, no. 3, pp. 127–138, Sep. 2013.
[31] J. Sun, "On the zero-crossing distortion in single-phase PFC converters," *IEEE Trans. Power Electron.*, vol. 19, no. 3, pp. 685–692, May 2004.
[32] S. Sivakumar, K. Natarajan, and R. Gudelewicz, "Control of power factor correcting boost converter without instantaneous measurement of input current," *IEEE Trans. Power Electron.*, vol. 10, no. 4, pp. 435–445, Jul. 1995.
[33] V. M Rao, A. K. Jain, K. K Reddy, and A. Behal, "Experimental comparison of digital implementations of single-phase PFC controllers," *IEEE Trans. Ind. Electron.*, vol. 55, no. 1, pp. 67–78, Jan. 2008.

Sung Min Park (S'10–M'15) received the B.S. degree in electronics engineering and the M.S. degree in electrical engineering from Korea University, Seoul, Korea, in 2001 and 2003, respectively. He is currently working toward the Ph.D. degree at the Department of Electrical and Computer Engineering, University of Connecticut, Storrs, CT, USA.

From 2003 to 2008, he was a Senior Engineer with LG Electronics, Seoul. From 2008 to 2010, he was with Samsung Heavy Industries, Suwon, Korea. From 2014, he is a Senior Research Engineer at the United Technologies Research Center, East Hartford, CT. His research interests include power electronics applications for home appliances and renewable energy systems.

Sung-Yeul Park (S'04–M'09) received the M.S. and Ph.D. degrees in electrical and computer engineering from Virginia Polytechnic Institute and State University, Blacksburg, VA, USA, in 2004 and 2009, respectively.

From 2002 to 2004, he was a Graduate Research Assistant with the Center for Rapid Transit Systems, Virginia Tech. From 2004 to 2009, he was a Graduate Research Assistant with the Future Energy Electronics Center, Virginia Tech. He joined the Department of Electrical and Computer Engineering, University of Connecticut, Storrs, CT, USA, as an Assistant Professor, and as an Associate Member of the Center for Clean Energy Engineering in 2009. His research interests include efficient energy and power conversion, renewable and distributed generation integration, smart buildings, and microgrid applications.

Dr. Park has received several international paper awards including a Best Paper Award at the IEEE Power Conversion Conference in 2007, and an Outstanding Writing Award in the International Future Energy Challenge in 2007.